JOURNAL OF AIRCRAFT
Vol. 43, No. 1, January–February 2006

Extensions of Overset Unstructured Grids to Multiple Bodies in Contact

Fumiya Togashi,* Yasushi Ito,* Kazuhiro Nakahashi,† and Shigeru Obayashi‡
Tohoku University, Sendai 980-8579-01, Japan

The overset unstructured grid method is extended to multiple bodies that are in contact with each other, and the treatment of nodes in the overlapping regions of two bodies in contact is discussed in detail. The developed overset unstructured grid method is applied to the following cases: ONERA M5 body/wing, ONERA M6 store separation, and the National Aeronautical Laboratory (NAL) experimental supersonic airplane/booster separation. In each case, there are two bodies in contact, and the calculation is performed with the Euler code. The calculation results clearly show smooth transitions of the contour lines between two bodies. In the ONERA M6 and NAL airplane/booster cases, a simulation of separation from the connecting configuration is performed.

Introduction

TO handle complex and moving-body problems, the overset grid approach, where several structured grids overlap and cover the flowfield, was introduced by Steger et al.[1] and Benek et al.[2] This approach is so powerful that remeshing is not required even for moving bodies. However, it also has several shortcomings, such as a loss of conservation, extra costs due to interpolation, and locally reduced accuracy due to mismatched grid sizes. The most critical issue of the conventional overset structured grid approach is the complexity of the procedure. As the complexity of the geometry increases, the required number of overlapping grids increases. This causes difficulty in constructing the information necessary for communication among grids and requires more time-consuming work. These difficulties may have hindered the wide application of the method in industry.

The overset unstructured grid method has been proposed by the present authors and successfully applied to several problems.[3–5] The approach has also been employed in other studies.[6,7] In those studies, the method showed good performance when used to solve complicated, moving-bodies problems. The unstructured grid has great flexibility in handling complex geometries. When unstructured meshes are used for the overset concept, the number of submeshes required for covering the flowfield can be significantly reduced as compared with that needed in the case of overset structured grid. As a result, generating interpolation stencils between grids becomes simple. It can also extend the applicability of the unstructured grid method to multiple moving-body problems without a serious effort in the code development for a deforming mesh and remeshing procedure.

There is, however, still room for improvement of the overset unstructured grid method, for example, in the treatment of multiple bodies that are in contact with each other. A typical example of the problem is store separation, where a store is first attached to the fuselage or wing and then released. Another use is for design, for example, to find an optimum location of a nacelle/pylon on a wing, a flow simulation around a complete airplane must be performed by changing the position of the nacelle. This necessitates a troublesome procedure to generate a grid for each different position of the nacelle if a single grid is used to cover the entire configuration. Instead, this procedure can be simplified if overset grids are used. For this case, two grids, one for the wing/fuselage and the other for the nacelle/pylon, cover the entire flowfield, and a parametric study of the nacelle location for optimization can be performed easily and efficiently in a single flow computation without remeshing.

Another problem is to estimate accurately the best-balanced locations of the aerodynamic center and the center of gravity. In such a problem, a simulation in which the location of the wing is changed can be easily performed using this approach. Even in a conceptual design, where the panel method or linear theory is conventionally used, calculations of the Euler code are more effective in the case of a transonic airplane, which requires treatment of a shock wave. When this approach is used, performance of surface mesh regeneration due to the change of the position of the parts can be avoided, and the time needed for the design can be dramatically reduced. As a result, the design period of a new airplane becomes much shorter.

In this paper, a method for treatment of multiple bodies that are in contact with each other is discussed mainly as an extension of the overset unstructured grid concept. Test cases are presented, which include the ONERA M5 body/wing configuration, store separation, and the NAL experimental supersonic airplane/booster separation.

Overset Procedure

The identification of the intergrid boundary in multiple-body problems must be performed completely automatically to take advantage fully of the overset unstructured grid approach. The efficiency and robustness of the hole-cutting procedure are particularly important for moving-body problems. Here the wall distance is used as a basic parameter to construct the intergrid boundary. Node points that are closer to the wall boundary of their own grid are defined as a calculating field.[3,4]

Let us consider an example of the hole-cutting procedure. In Fig. 1, suppose that the broken lines show the grid (grid A) generated around body A and that the solid lines show (grid B) for body B. Node ***i*** belongs to grid A, and then the donor cell in grid B is indicated by a–b–c in Fig. 1. The minimum wall distance of this node ***i*** to body A is compared with the wall distance of the donor cell to body B. The distance of the donor cell is evaluated by a linear interpolation from its vertex values. Because the wall distance of node ***i*** to body A is shorter than that of donor cell a–b–c to body B, node ***i*** is assigned as an active node. (It belongs to the computational field.) In contrast, node ***j*** in Fig. 1 is designated as a nonactive node. In this way, all node points in the overlapping region are assigned as active (computational) or nonactive (noncomputational) nodes.

Presented as Paper 2002-2809 at the AIAA 20th Applied Aerodynamics Conference, St. Louis, MO, 25 June 2002; received 20 January 2003; revision received 30 July 2003; accepted for publication 30 July 2003.

*Graduate Student, Department of Aerospace Engineering, Aoba-ku Aramakiaza Aoba 01.

†Professor, Department of Aerospace Engineering, Aoba-ku Aramakiaza Aoba 01. Associate Fellow AIAA.

‡Associate Professor, Institute of Fluid Science, Aoba-ku Aramakiaza Aoba 01. Associate Fellow AIAA.

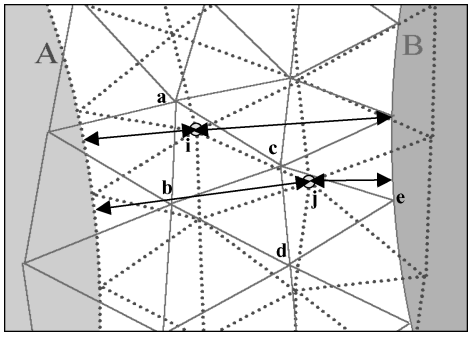

Fig. 1 Determination of intergrid boundary between grids: . . . , grid A and ——, grid B.

Flow Solver

In the present method, the computational domain consists of several unstructured subgrids, which may overlay each other. The unstructured subgrids generated around each component in the flowfield are put together to discretize the whole computational domain. The Euler equations are solved in each subgrid with the proper boundary conditions.

The Euler equations for compressible inviscid flows are written in an integral form as follows:

$$\frac{\partial}{\partial t}\int_{\Omega} \boldsymbol{Q}\,\mathrm{d}\boldsymbol{V} + \int_{\partial\Omega} \boldsymbol{F}(\boldsymbol{Q})\cdot\boldsymbol{n}\,\mathrm{d}\boldsymbol{S} = 0 \tag{1}$$

where $\boldsymbol{Q} = [\rho, \rho\boldsymbol{u}, \rho\boldsymbol{v}, \rho\boldsymbol{w}, \boldsymbol{e}]^T$ is the vector of conservative variables: ρ is the density; u, v, and w are the velocity components in the x, y, and z directions; and e is the total energy. The vector $\boldsymbol{F}(\boldsymbol{Q})$ represents the inviscid flux vector, and $\boldsymbol{n}$ is the outward normal of $\partial\Omega$, which is the boundary of the control volume Ω. This system of equations is closed by the perfect gas equation of state.

The equations are solved by a finite volume cell-vertex scheme. The control volume is a nonoverlapping dual cell. For the control volume, Eq. (1) can be written in an algebraic form as

$$\frac{\partial \boldsymbol{Q}_i}{\partial t} = -\frac{1}{\boldsymbol{V}_i}\sum_{j(i)} \Delta\boldsymbol{S}_{ij}\boldsymbol{h}\left(\boldsymbol{Q}_{ij}^{+}, \boldsymbol{Q}_{ij}^{-}, \boldsymbol{n}_{ij}\right) \tag{2}$$

where $\Delta\boldsymbol{S}_{ij}$ is the segment area of the control volume boundary associated with the edge connecting points $\boldsymbol{i}$ and $\boldsymbol{j}$. This segment area, $\Delta\boldsymbol{S}_{ij}$, as well as its unit normal $\boldsymbol{n}_{ij}$, can be computed by summing up the contribution from each tetrahedron sharing the edge. The term $\boldsymbol{h}$ is an inviscid numerical flux vector normal to the control volume boundary, and $\boldsymbol{Q}_{ij}^{\pm}$ are values on both sides of the control volume boundary. The subscript of the summation, $\boldsymbol{j}(\boldsymbol{i})$, represents all node points connected to node $\boldsymbol{i}$.

The numerical flux $\boldsymbol{h}$ is computed using the approximate Riemann solver of Harten–Lax–van Leer–Einfeldt–Wada (see Ref. 8). Second-order spatial accuracy is realized by a linear reconstruction of the primitive gasdynamic variables with Venkatakrishnan's limiter.[9]

The lower/upper symetric Gauss–Seidel (LU-SGS) implicit method (see Ref. 10) is applied to integrate Eq. (2) in time. With $\Delta\boldsymbol{Q} = \boldsymbol{Q}^{n+1} - \boldsymbol{Q}^{n}$ and a linearization of the numerical flux term as $\boldsymbol{h}_{ij}^{n+1} = \boldsymbol{h}_{ij}^{n} + \boldsymbol{A}_i^{+}\Delta\boldsymbol{Q}_i + \boldsymbol{A}_j^{-}\Delta\boldsymbol{Q}_j$, the final form of the LU-SGS method on an unstructured grid becomes for the forward sweep

$$\Delta\boldsymbol{Q}_i^{*} = \boldsymbol{D}^{-1}\left[\boldsymbol{R}_i - 0.5\sum_{j\in L(i)} \Delta\boldsymbol{S}_{ij}\left(\Delta_j^{*} - \rho_A\Delta_j^{*}\right)\right] \tag{3a}$$

and for the backward sweep

$$\Delta\boldsymbol{Q}_i = \Delta\boldsymbol{Q}_i^{*} - 0.5\boldsymbol{D}^{-1}\sum_{j\in U(i)} \Delta\boldsymbol{S}_{ij}(\Delta\boldsymbol{h}_j - \rho_A\Delta\boldsymbol{Q}_j) \tag{3b}$$

where

$$\boldsymbol{R}_i = -\sum_{j(i)} \Delta\boldsymbol{S}_{ij}\boldsymbol{h}_{ij}^{n}, \qquad \Delta\boldsymbol{h} = \boldsymbol{h}(\boldsymbol{Q}+\Delta\boldsymbol{Q}) - \boldsymbol{h}(\boldsymbol{Q})$$

and $\boldsymbol{D}$ is a diagonal matrix derived by the Jameson–Turkel[11] approximation of the Jacobian as $\boldsymbol{A}^{\pm} = 0.5(\boldsymbol{A} \pm \rho_A\boldsymbol{I})$, where ρ_A is the spectral radius of Jacobian $\boldsymbol{A}$. $\boldsymbol{D}$ is given as follows:

$$\boldsymbol{D} = \left(\frac{\boldsymbol{V}_j}{\Delta t} + 0.5\sum_{j(i)} \Delta\boldsymbol{S}_{ij}\rho_A\right)\boldsymbol{I} \tag{4}$$

The lower/upper splitting of Eq. (3), namely, $\boldsymbol{j}\in\boldsymbol{L}(\boldsymbol{i})$ and $\boldsymbol{j}\in\boldsymbol{U}(\boldsymbol{i})$, for the unstructured grid is realized by using a grid reordering technique[10] to improve the convergence and the vectorization.

Overset Implementation

In addition to the boundaries of the computational domain, subgrids may have holes and intergrid boundaries with the neighboring donor subgrids. The node points belonging to the noncomputational field must be excluded or blanked out of the flowfield solution. All node points have information as to whether they belong to the computational field or not, namely,

$$\boldsymbol{I}\mathrm{BLANK} = \begin{cases} 1, & \text{the point is not a blanked out node.} \\ 0, & \text{the point is a blanked out node} \end{cases}$$

This value is 1 or 0 depending on the area inside or outside the computational subregion. In the flow solver, the right-hand-side vector $\boldsymbol{R}_i$ in Eq. (3) is multiplied by the value $\boldsymbol{I}\mathrm{BLANK}(\boldsymbol{i})$, namely, the variables in the outside region (hole region) are temporarily set to be zero. First each grid is calculated, and then flow variables are interpolated around the intergrid boundary. If a node whose $\boldsymbol{I}\mathrm{BLANK}$ is 0 has a partner cell that belongs to the computational field, the node is interpolated from the flow variables of the partner cell. That is, the node of $\boldsymbol{I}\mathrm{BLANK} = 0$ is never calculated, although it has the flow variables given by its partner grid. Because of this procedure, computational accuracy around the intergrid boundary is highly improved.

Treatment of Multiple Bodies in Contact

A similar procedure can be applied to multiple bodies in contact. The procedure is shown in Fig. 2 and can be explained as follows. In Fig. 2, node point A (circular shaped) belongs to body 1 (light gray zone) and node points a, b, and c and the other square-shaped and diamond-shaped points belong to body 2 (dark gray zone). Solid lines show the mesh generated around body 2 and dotted lines show the mesh of the wall boundary:

1) Node points that are located inside another body, for example, diamond-shaped node points that are located inside body 1, have their $\boldsymbol{I}\mathrm{BLANK}$ set to 0.

2) Check all edges: If one node point is located in the flowfield, for example, square-shaped node points, and the other is located inside a body, the wall boundary condition is applied to the edge. The node point that is located inside the body is given the density and pressure of the opposite node point, whereas the velocity is defined to realize the slip condition between the two node points.

3) If the node points that are inside a grid body do not have a neighboring node point in the flowfield, the nodes are interpolated

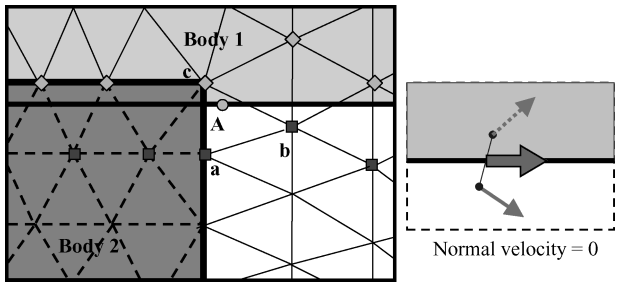

Fig. 2 Treatment of multiple bodies in contact.

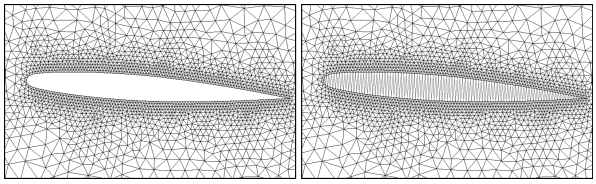

Fig. 3 Inner mesh, which is the mesh generated inside the body.

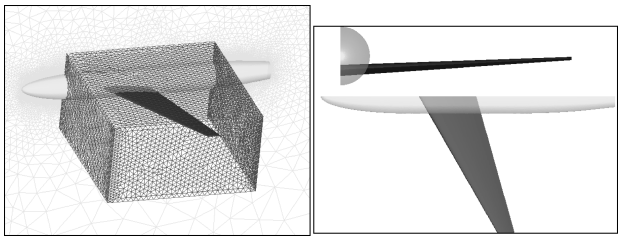

Fig. 4 Overset unstructured grids for the ONERA M5 wing/fuselage.

from the flow variables from the super triangle that is the mesh generated inside the body (Fig. 3).

4) Because of the described treatment, node point c has some nonzero flow variables, and node point A obtains adequate flow variables from the interpolation of the partner-cell a–b–c.

The procedure mentioned is important for a separating simulation. Originally, the inner mesh is generated for-fast and accurate search for the partner cell, and thus, the search can pass through the inside of the body. However, the inner mesh is a very important factor for problems of separation. The node points that are inside the body (namely, the partner cell belongs to the inner mesh) have proper variables so they can be calculated even when they node points enter the calculating field during the separation.

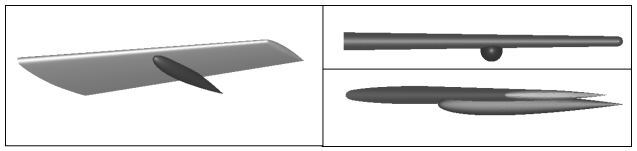

Fig. 7 ONERA M6 wing and dropping tank configuration.

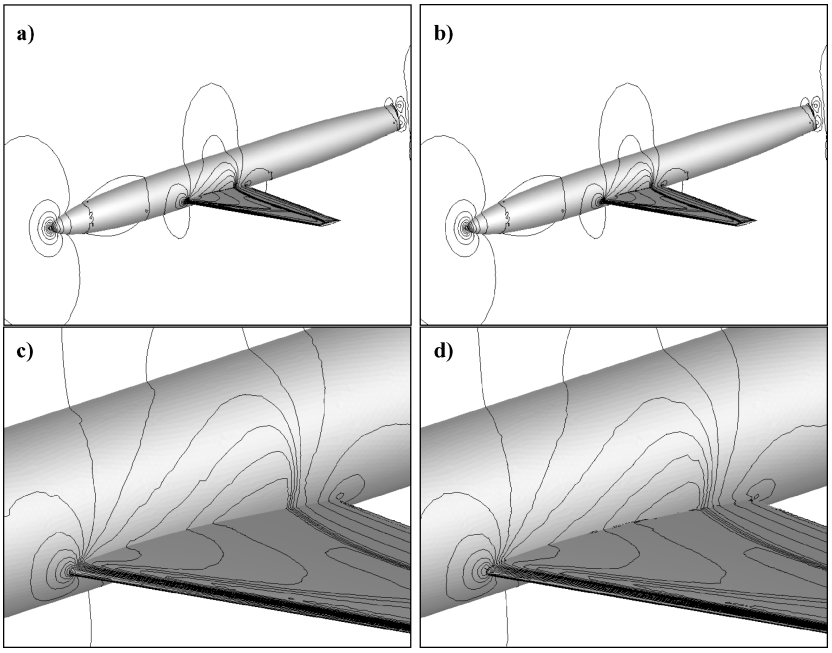

Fig. 5 Computed pressure contours on the surface and symmetrical plane for the ONERA M5 wing/fuselage $M_\infty = 0.84$ and $\alpha = -1.0$ deg: a) and c) single grid case and b) and d) overset grid case.

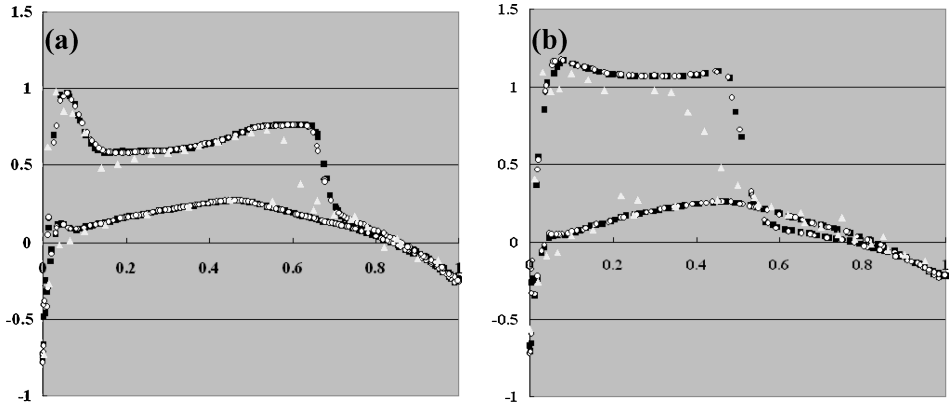

Fig. 6 Comparison of C_p distributions for the ONERA M5 at $M_\infty = 0.84$ and $\alpha = -1.0$ deg at semispan locations of a) 20% and b) 85%: ○, overset grid; ■, single grid; and ▲, experiment.

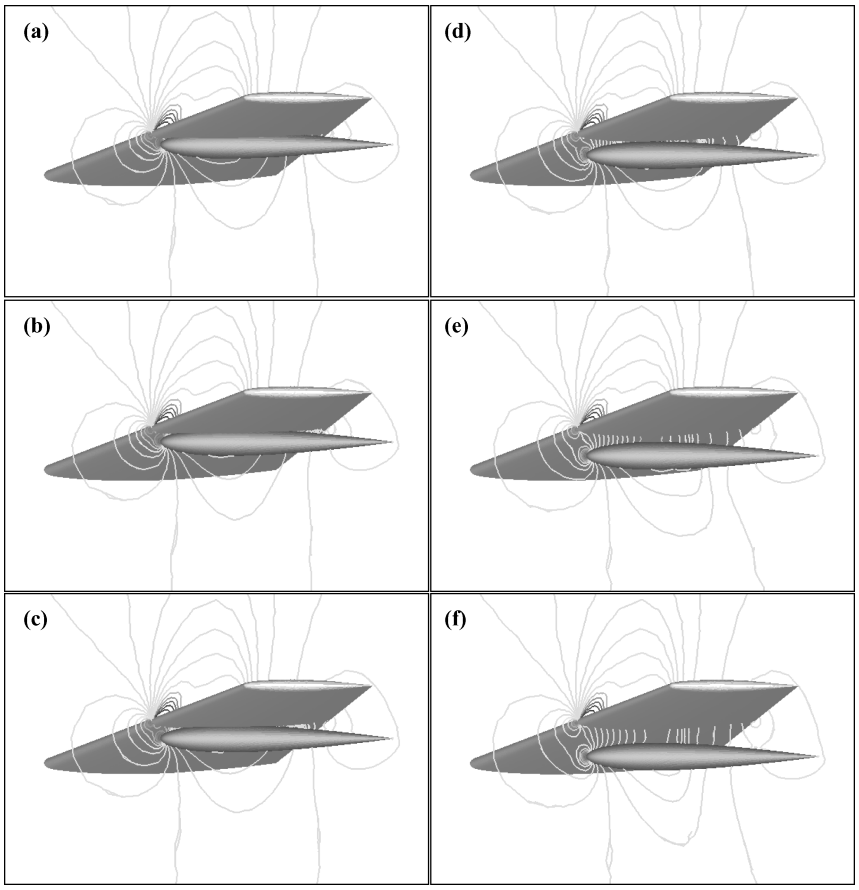

Fig. 8 Computed pressure contours between the wing and the tank, M_∞ = 0.84 and α = 3.06 deg.

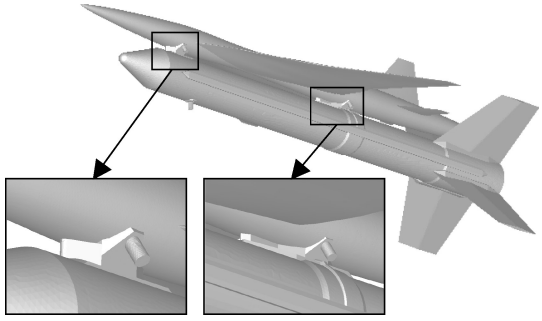

Fig. 9 NAL's experimental supersonic airplane with rocket booster for launch.

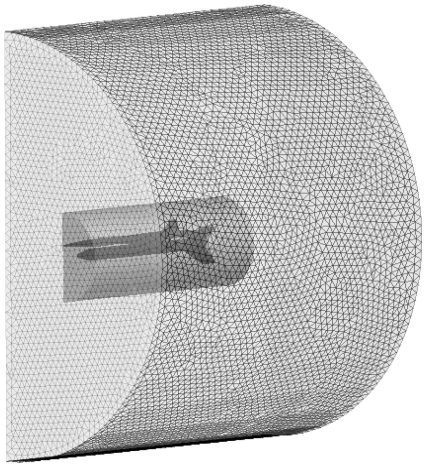

Fig. 10 Overset grids for the supersonic airplane (outer cylindrical region) and the rocket booster (inner cylindrical region).

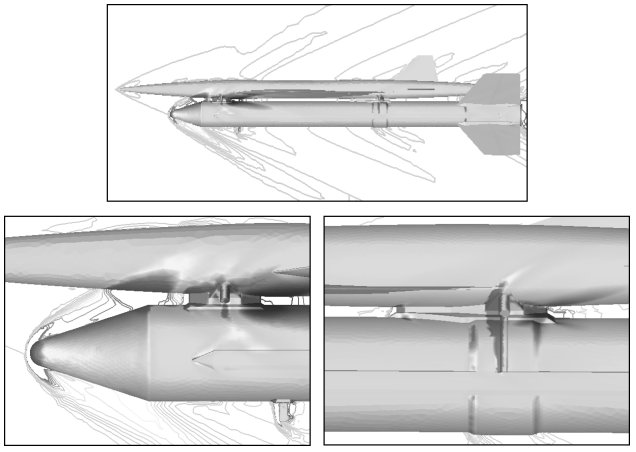

Fig. 11 Pressure contours on the surface and symmetrical plane of the supersonic airplane rocket booster at freestream M_∞ = 2.5 and α = 0.0 deg.

Computational Results

ONERA M5

The ONERA M5 wing/fuselage configuration is considered as a test case of this approach. First, a single hemispherical grid that covers the entire flowfield was generated. For a test of the overset grid, a box-shaped subregion that covers only the near field of the wing was defined as shown in Fig. 4, and a relatively fine tetrahedral grid was generated in it. The surface grid on the fuselage is the same as that used for the hemispherical grid. The intergrid boundaries between these grids were identified using the distances from the wing surface for the box grid and from the outer boundary for the hemispherical grid. With this approach, the cells in the box grid are

preserved, whereas the near-field cells in the hemispherical grid are automatically blanked out for computations.

The computations were performed using both the single hemispherical grid and the overset grids for a freestream Mach number of 0.84 and an angle of attack of −1 deg. Figure 5 shows the computed pressure contours for the case of a single grid (Figs. 5a, and 5c) and that of overset grids (Figs. 5b and 5d). In Figs. 5b and 5d, smooth transitions of the contour lines between the wing and the fuselage boundary can be observed. Figure 6 shows comparisons of the C_p distributions in the case of overset grids, that of a single grid and the experimental data on the wing at 20 and 85% semispan locations.[12] The results show good agreement between the overset grid case and the single grid case. The difference of the location of the second shock wave between the calculation and the experiment is due to the calculation performed by the Euler code.

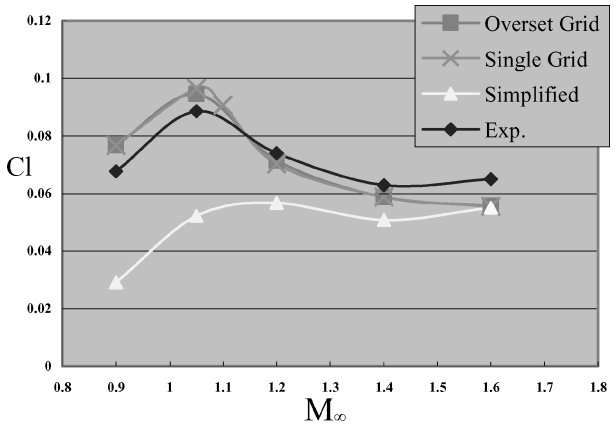

Fig. 12 Comparison of the C_l of the airplane and the booster at various Mach numbers.

Dropping Tank

For a test case of a store separation, a wing from which a tank is dropped was simulated. The upper part of the dropping tank is embedded in the wing at the beginning (Fig. 7), then the tank moves downward. The wing configuration is the ONERA M6 wing.[13] The dropping tank is a body of revolution made from an NACA0012 airfoil. The movement of the tank was prescribed. Figure 8 shows the pressure contours between the wing and the tank. Smooth transitions of the contour lines between the bodies can be observed.

Experimental Supersonic Airplane with a Booster

Figure 9 shows configurations of an experimental supersonic airplane and a booster of the National Aerospace Laboratory (NAL) of Japan. The fuselage length of the airplane is 11.5 m, and the span is 4.718 m. The experimental airplane was designed to realize the laminar boundary layer on the forward part of the wing. The airplane will be launched by a solid rocket booster to an altitude of 15,000 m at a Mach number of 2.5. For the configuration shown in Fig. 9, two unstructured grids, each of which covers the airplane and the

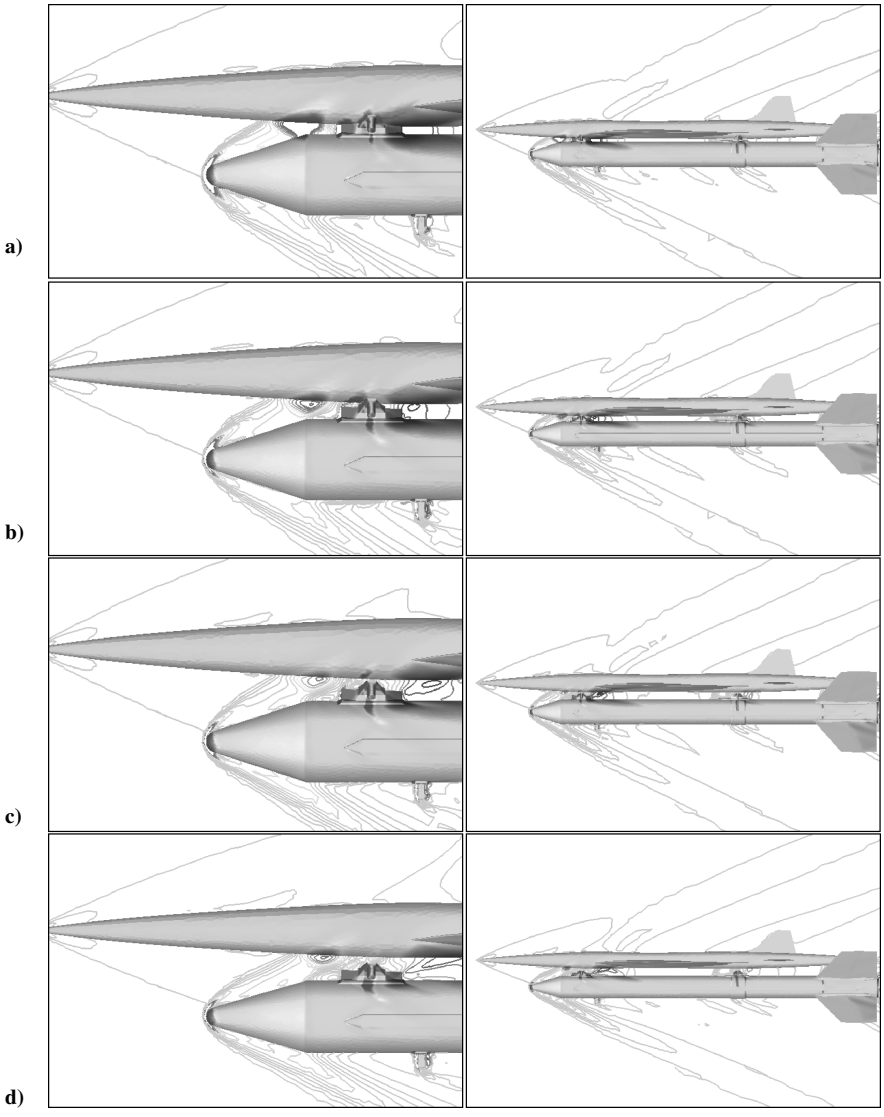

Fig. 13 Separating calculation results: pressure contours of the airplane/rocket booster at freestream M_∞ = 2.5 and α = 0.0 deg.

rocket booster, were generated as shown in Fig. 10. Because of the unstructured meshes, even the connecting parts of the booster were successfully described by one unstructured grid. An outer cylindrical grid was generated for the airplane, and an inner cylindrical grid was generated for the rocket booster.

The connecting parts of the rocket booster are first embedded in the lower surface of the experimental airplane, and then separation of the booster begins. The movement is subject to gravity, and other forces are not considered. Figure 11 shows calculated pressure distribution results before the beginning of the separation. The results show the complex reflection shock wave patterns between the two bodies. The effect of the connecting parts between the bodies is clearly observed. A shock wave is generated from the connecting parts and impinges on the lower surface of the wing of the airplane. Figure 12 shows a comparison of the C_L of the airplane with the booster installed at various Mach numbers. In Fig. 12, the data of "Simplified" shows the C_L of an airplane with a booster without connecting parts between the bodies. Figure 12 shows the significance of the connecting parts for the successful simulation, especially around the transonic region. Figure 13 also shows pressure distribution results during the separation. As shown in Fig. 13, the calculation is successfully performed even when the booster is released from the airplane.

In the experimental airplane/booster separation, the location of the booster is also a very important factor for the success of the experiment. The change of the location of the booster has an effect on the aerodynamic force of the airplane, resulting in a difference between the center of gravity and the aerodynamic center. Such a difference will effect the moment of the airplane after the separation. By this approach, successive calculations changing the location of the booster becomes possible without regenerating new meshes for the airplane and the booster.

Conclusions

The overset unstructured grid method was extended to multiple bodies in contact. With use of the ONERA M5 wing/fuselage configuration, the method was validated by comparison between the overset grid case and the single grid case. The dropping tank case shows the capability of the store separating simulation in which the store is embedded in the wing at the beginning. Finally, the method was applied to the NAL experimental supersonic airplane/booster separation case. Even though these two bodies have very complicated configurations, it was possible to use only one unstructured mesh to describe each body. The calculating results successfully predict the complex reflection shock wave patterns between the two bodies.

By this approach, successive calculations with changes in the location of the booster become possible without regenerating new meshes of the airplane and the booster. Such calculations are very useful to estimate the best position of the booster for launch configuration. Because of this, this method will be a powerful tool not only for store separation but also for airplane design.

Acknowledgments

The authors would like to thank the Aerodynamic Design Group of the Next Generation Supersonic Transport Project Center, the National Aerospace Laboratory of Japan, for providing us with the geometry data of the airplane. We also would like to thank T. Fujita, a graduate student of Tohoku University, for his help in generating the STL (stereolithography) data for the surface grids.

References

[1]Steger, J. L., Dougherty, F. C., and Benek, J. A., "A Chimera Grid Scheme," *Proceedings of the American Society of Mechanical Engineers Mini-Symposium on Advances in Grid Generation*, 1982.

[2]Benek, J. A., Buning, P. G., and Steger, J. L., "A 3-D Chimera Grid Embedding Technique," AIAA Paper 85-1523, 1985.

[3]Nakahashi, K., Togashi, F., and Sharov, D., "Intergrid-Boundary Definition Method for Overset Unstructured Grid Approach," *AIAA Journal*, Vol. 38, No. 11, 2000, pp. 2077–2084.

[4]Togashi, F., Nakahashi, K., Ito, Y., Shinbo, Y., and Iwamiya, T., "Flow Simulation of NAL Experimental Supersonic Airplane/Booster Separation," *Computers and Fluids*, Vol. 30, No. 6, 2001, pp. 673–688.

[5]Togashi, F., Ito, Y., Murayama, M., Nakahashi, K., and Kato, T., "Flow Simulation of Flapping Wings of An Insect Using Overset Unstructured Grid," *CFD Journal*, Vol. 12, No. 1, pp. 98–106.

[6]Lohner, R., Sharov, D., Luo, H., and Ramamurti, R., "Overlapping Unstructured Grids," AIAA-2001-0439, 2001.

[7]Luo, H., Sharov, D., and Baum, J. D., "An Overlapping Unstructured Grid Method for Viscous Flows," AIAA-2001-2603, 2001.

[8]Obayashi, S., and Guruswamy, G. P., "Convergence Acceleration of an Aeroelastic Navier–Stokes Solver," AIAA Paper 94-2268, 1994.

[9]Venkatakrishnan, V., "On the Accuracy of Limiters and Convergence to Steady State Solutions," AIAA Paper 93-0880, Jan. 1993.

[10]Sharov, D., and Nakahashi, K., "Reordering of Hybrid Unstructured Grids for Lower–Upper Symmetric Gauss–Seidel Computations," *AIAA Journal*, Vol. 36, No. 3, 1998, pp. 484–486.

[11]Jameson, A., and Turkel, E., "Implicit Schemes and LU Decompositions," *Mathematics of Computation*, Vol. 37, No. 156, 1981, pp. 385–397.

[12]*Proceedings of the 10th NAL Symposium on Aircraft Computational Aerodynamics*, 1992.

[13]Schmitt, V., and Charpin, F., "Pressure Distributions on the ONERA M6-wing at Transonic Mach Numbers," *Experimental Data Base for Computer Program Assessment*, AGARD AR-138, 1979.